19 Dendritic Integration in a Two-Neuron Recurrent Excitatory Network Model

Roman R. Poznanski

CONTENTS

19.1 Introduction

The most advanced neural network models include "spiking" neuron models (also referred to as conductance-based point neuron models or integrate-and-fire models) as single isopotential compartments (i.e., without spatial structure) that fire impulses whenever a voltage threshold is exceeded. Although the field is slowly undergoing reform, these "spiking" neurons are still being used in many network models (e.g., see Gerstner and Kistler, 2002). However, if dendritic structure is taken into consideration, then axodendritic synaptic connections may not reliably evoke impulses when stimulated, due to the cable properties of dendrites and the sparse distribution of voltage-dependent ionic channels as shown by *ionic cable theory* (Poznanski, 2001b). Therefore, to adequately represent dendritic integration, it is vital to construct neuronal networks as biologically constrained models, focusing on the inclusion of the relevant physicochemical processes. Such an approach to modeling in the neurosciences urgently needs to be developed.

In the past, the status quo for modeling active dendrites was to assume fully active Hodgkin–Huxley-like channel kinetics in a network of multicompartmental models (Gardner, 1993; Lansner and Fransen, 1995; Bibbig et al., 2002; Nenadic et al., 2003). The problem with such models is their inability to link hierarchical neuronal structures (at the subcellular, cellular, and network level) in a practical manner. For instance, in the words of Traub and Jefferys (1994, p. 116): "others have

modeled individual neurons with many thousands of compartments, but such models do not lend themselves to network simulations." Most often multicompartmental models of single neurons are reduced ranging from a single to a dozen compartments for practical purposes leaving the validity of the approach in question. Invariably a multicompartmental model representation of a single neuron is inept at advancing to the network level in an efficient way because of the sheer complexity in terms of the thousands of parameters it has required to adequately represent a single neuron, as for example, exemplified by Spruston and Kath (2004):

> One strategy for developing more sophisticated neural networks is to replace simple elements with sophisticated computational models of neurons, including branching dendritic trees, thousands of synapses, and dozens of voltage-gated conductances. The problem with this approach is that it is not manageable to use such computationally expensive neuronal models in large-scale networks.

The need to construct integrative as opposed to computational neural models of networks is therefore fundamental to new advances in our understanding of dendritic integration.

All multicompartmental models suffer from the nonuniqueness problem (Rall, 1990, 1995a). Therefore the lack of robustness of such models to parameter changes could in principle be the most significant cause of variability in response characteristics. This often overlooked anomaly adds emphasis to the conclusion found by Krichmar et al. (2002), that altered morphology per se (keeping all other factors constant) drastically modified the spiking activity of their simulated multicompartment hippocampal neurons. Our aim is to show that changes in the distribution of ionic channels and numerous other nonmorphological parameters can also bring about major changes in response characteristics. Unequivocally, compartmentalization of the neuronal membrane, by which the continuous nature of the neuronal membrane is sliced to pieces, introduces discontinuities that are not intrinsic to real neuronal circuitry. For instance, Calabrese et al. (2000) offer a basic modeling strategy for small-scale neural networks which "boils down" to solving the following current balance equation for any whole single-compartment neuron model or any single compartment within a multicompartment neuron model:

$$C\,\mathrm{d}V/\mathrm{d}t = -\sum(I_{\mathrm{ion}}) - \sum(I_{\mathrm{syn}}) + \sum(I_{\mathrm{inject}}),$$

where I_{ion} represents membrane currents (e.g., voltage-gated and leak currents), I_{syn}, synaptic currents, and I_{inject}, injected currents (or the current from connected compartments). This equation is used without comment in almost all software packages. The work presented here, however, suggests that it will be important in new models of neurons in networks to incorporate wherever possible a continuously distributed spatial structure.

A significant challenge in the construction of biophysically realistic neurons in networks is to identify and incorporate the cellular behavior in the mathematical description of the macroscopic population behavior. We have developed a model for a recurrent excitatory network of two "weakly" active neurons from the result of a *subthreshold* current injection into a point close to the fictitious soma of one neuron. Such modeling is new because recurrent network models with a distributed dendritic structure (see Bressloff, 1995, 1996, 1999; Bressloff and Coombes, 1997a, 1997b; Coombes and Lord, 1997; Bressloff and De Souza, 1998) were developed without any voltage-dependent ionic channels. We propose to show, using a two-neuron recurrent excitatory network model, that "weakly" excitable dendrites enable the dendritic spike to propagate passively along its arbor, without too much decrement in its amplitude if the spatial distribution between clusters (or hot spots) of voltage-dependent ionic channels is small, approximating an almost uniform-density distribution of voltage-gated ion channels. We also aim to show how feedback in a system of two neurons can maintain peak amplitude in the postsynaptic neuron at a distally placed location along the dendrite. This is important because experimental studies showing that somatic feedback to the dendrites becomes

stronger with increasing network activity (Waters and Helmchen, 2004) are incapable of showing the effect on distal fine dendrites.

19.2 Ionic Cable Theory for Conduction of Dendritic Potentials

19.2.1 Ionic Cable Equation for a Single Neuron

Let V be the depolarization (i.e., membrane potential less than the resting potential) in mV, and I_{ion} be the inward ionic-current density through the membrane enclosing a unit length of cable (i.e., per unit membrane surface of cable [mA/cm]), as defined in Section 19.2.2. The voltage response or depolarization as a result of synaptic input, as defined in Section 19.2.4, in a leaky cable representation of a cylindrical passive dendritic cable with I_{ion} occurring at discrete points, that is, $x = x_{\text{p}}$, can be shown to satisfy:

$$C_{\text{m}}V_t = \left(\frac{d}{4R_{\text{i}}}\right)V_{xx} - \frac{V}{R_{\text{m}}} - \sum_{j=1}^{N} I_{\text{ion}}(x,t;V)\,\delta(x-x_j) - \sum_{k=1}^{M} g(t)[V - V^{\text{rev}}]\delta(x-x_k)$$
$$- \sum_{z=1}^{N} P\delta(x-x_z), \quad t > 0, \tag{19.1}$$

where x is the distance (cm), t is time (sec), d is the diameter of the cable (cm), C_{m} is the membrane capacitance (F/cm^2), R_{m} is the membrane resistivity (Ω cm^2), R_{i} is the intracellular resistivity (Ω cm), N is the number of hot spots of voltage-dependent ionic channels, M synapses control the ionic channels at specified positions along the dendritic cable (i.e., $x = x_k$), with time-dependent conductance changes $g(t)$ (S/cm) and reversal potentials V^{rev} (mV). P is the sodium-pump current density representing ion fluxes due to active transport (mA/cm), and δ is the Dirac delta function reflecting the position on the membrane where the ionic current is represented along the circumference of the cable per cm. Subscripts x and t indicate partial derivatives with respect to these variables, and by convention, inward current is negative and outward current is positive.

19.2.2 Representation of Noninactivating Voltage-Dependent Ionic Currents

The integration of synaptic signals in dendrites has been shown experimentally to be affected by persistent Na^+ (Na^+P) channels, resulting in amplified synaptic potentials (see MacVicar, 1985; Schwindt and Crill, 1995; Stuart and Sakmann, 1995; Lipowsky et al., 1996; Urban et al., 1998; Fricker and Miles, 2000; Berman et al., 2001; Gonzalez-Burgos and Barrionuevo, 2001; Koizumi et al., 2001) as well as enhancement of backpropagating action potentials (bAPs) (Pan and Colbert, 2001; Doiron et al., 2003). The spatial location and distribution of Na^+ channels in dendrites remains unknown, yet several studies have shown a high differential in the densities of sodium channels along axonal and dendritic membranes (Safronov, 1999). Furthermore, it is safe to assume that Na^+P channels are present in low density (about 2% of the Na^+ channels) and make the membrane "weakly" excitable to support a nonregenerative dendritic spike in the subthreshold voltage range.

Dendritic spikes are mediated predominately by Na^+ channels, although K^+ channels have been found in some dendrites (see Hoffman et al., 1997). Thus, the experimental observation of peak amplitude reduction of backpropagating dendritic spikes could be due to a sparse density of Na^+ channels or to a high concentration of K^+ ions in the extracellular medium pointing indirectly to the presence of K^+ channels on dendrites (cf. Johnston et al., 1999). It

is well known that Na^+ channels may be induced to lose their capability for inactivation as a result of chemical treatments or exposure to proteolytic enzymes (e.g., protease and papaine), yet these treatments have a relatively minor or no effect on activation in these channels. When Na^+ channels lose inactivation, Na^+ currents show no inactivation; persistent currents without transient components are a common occurrence for freshly dissociated cells (cf. Poznanski, 2001d).

The inward ionic-current density per unit membrane surface of the cable (mA/cm) may be represented as

$$I_{\text{ion}}(x,t;V) = g_{\text{ion}}m(V)[V - V_{\text{ion}}], \quad t > 0, \tag{19.2}$$

where $V_{\text{ion}} = E_{\text{ion}} - E_{\text{r}}$, E_{r} is the resting membrane potential, E_{ion} is the equilibrium potential (mV), and g_{ion} (S/cm) is the conductance per unit membrane length of the cable obtained by multiplying the maximum attainable conductance of a single ionic channel by the number of channels contained in a unit length of cable. Note that the inward current in Equation (19.2) by convention is negative, which should not be confused with a current applied or injected via a pipette, which is positive because it is an intracellular current flowing outward. The dimensionless activation variable $m(V)$ is governed by a first-order reaction equation (Hodgkin and Huxley, 1952b):

$$\partial m/\partial t = \alpha_m(1 - m) - \beta_m m, \tag{19.3}$$

where α_m and β_m are the rate constants (in sec^{-1}) of the ionic channels independent of t. Equations (19.2) and (19.3) correspond to various *nonsynaptic* voltage- and time-dependent ionic currents.

19.2.3 Representation of Axodendritic Chemical Synapses

Modeling of synaptic transfer in artificial neural networks usually entails the inclusion of synaptic weights (see Kurogi, 1987; Seung et al., 2000), but real neuronal networks form axodendritic synapses that are activated by action potentials, resulting in a discrete or noncontinuous release of neural transmitters that leads to a change in conductance and subsequent generation of synaptic current in the postsynaptic neurons (see Miftakhov and Wingate, 1995). Modeling of this process is based on the following assumptions:

1. The rate of neural transmitter release is proportional to the activity of individual spikes arriving at the presynaptic terminals. Hence, to avoid the continuous representation of activity in terms of a mean firing rate, discrete spiking activity that releases neurotransmitter into the synaptic cleft can be included and used to investigate the consequences of the nonuniform firing of spikes. The rate of neural transmitter release depends upon the timing of the action potentials arriving at the presynaptic terminals, which can be represented by a series of Dirac delta functions:

$$E(V^{\text{pre}}) = \sum_{k=1}^{N_{\text{sp}}} \delta(t - t_k - \Delta t)\text{H}[V^{\text{pre}}(0,t) - \theta], \tag{19.4}$$

where N_{sp} is the total number of spikes, $t_k + \Delta t$ is the time of arrival of the kth spike at the synapse, where t_k is the time of generation of the spike at the soma or axon hillock and Δt is the axonal delay (sec), θ is the presynaptic threshold voltage, and $\text{H}[\cdot]$ is the Heaviside step function.

Equation (19.4) records a spike only if the presynaptic voltage is above the threshold. Hence, a spike may not be recorded for every measured time, especially for recurrent networks as discussed in Section 19.3.

2. The amount of neural transmitter release into the synaptic cleft is driven by the individual spike activity, which provides the source term in the first-order kinetic equation governing the amount of transmitter in the synaptic cleft. This process is often neglected and replaced by converting the presynaptic signal into postsynaptic activation via a conductance change based on first-order kinetics, as has been carried out by Wang et al. (see Golomb et al., 1994; Rinzel et al., 1998). The amount of neural transmitter in the synaptic cleft is given by:

$$\tau_c \, dC/dt = -C(t) + \tau_c C_0 E(V^{pre}), \tag{19.5}$$

where E is the input (presynaptic) spike-train activity (with dimension sec^{-1}) expressed through Equation (19.4), C_0 represents the maximum amount of transmitter (mM), and τ_c is the time constant of transmitter release in response to presynaptic depolarization (sec). It should be noted that in artificial neural networks, $C(t)$ is often ignored and replaced in Equation (19.6) with a source term represented as a series of Dirac delta functions for the conductance change (e.g., see Treves et al., 1996) because it is assumed that the duration of the neural transmitter release is sufficiently short (i.e., <1 msec) or the amount of neural transmitters in the synaptic cleft is sufficiently small, that $C(t)$ does not need to be temporally resolved (Chapeau-Blondeau and Chambert, 1995).

3. The neural transmitter–receptor channel kinetics obey a first-order process in which the synaptic conductance is assumed to be proportional to the total number of channels occupied by neural transmitter (Bernard et al., 1994), so the opening of the synaptic conductance is the product of the free neural transmitter and the number of unoccupied receptors, while the closing is determined by a simple exponential decay process (Leibovic and Sabah, 1969; Chapeau-Blondeau and Chambert, 1995). These kinetics lead to a complicated nonlinear equation for the time course of the synaptic conductance, which under most circumstances can be simplified to a damped harmonic oscillator equation (see Holmes and Levy, 1990; Bernard et al., 1994; Kalitzin et al., 1997; Rolls and Treves, 1998). More complex dynamics are necessary when neural transmitter–receptor kinetics are mediated by second messengers, such as a calcium influx (see Byrne and Gingrich, 1989). The following equation is based on first-order kinetics (Leibovic and Sabah, 1969; Chapeau-Blondeau and Chambert, 1995):

$$\tau_g \, dg/dt = -g(t) + \omega C(t)[g_{sat} - g(t)], \tag{19.6}$$

where τ_g is the time constant of the decay of $g(t)$ (sec), ω is the equilibrium constant for the neural transmitter–receptor interaction in mM^{-1}, g_{sat} $(= g_{max} M^*/\pi d)$ represents the saturating conductance associated with a noncontinuous release of neural transmitter per unit membrane surface of cable (S/cm), with g_{max} being the maximum conductance of an ionic channel (S), and $M^*/\pi d$ being the number of postsynaptic channels per unit membrane surface of cable. $C(t)$ is the amount of neural transmitter in the synaptic cleft (mM). The neural transmitters are released by the arrival of action potentials from the presynaptic neurons (cf. Hoppensteadt, 1986; Kurogi, 1987).

19.2.4 Network Equations without Synaptic Weights

Consider a recurrent excitatory network of two chemically coupled neurons with and without synaptic weights, as depicted in Figure 19.1. The first neuron, whose membrane potential is $V^0(x, t)$, provides

M synaptic inputs to the postsynaptic neuron, whose membrane potential is $V^1(x,t)$. Note that $U^0(x,t)$ reflects a quiescent neuron in the absence of synaptic activity and $V^0(x,t)$ reflects on the feedback from the synaptically coupled first neuron. The formulation of the system can be expressed in terms of the following equations:

$$C_m U_t^0 = \left(\frac{d_0}{4R_i}\right) U_{xx}^0 - \frac{U^0}{R_{m0}} - \sum_{j=1}^{N} I_{ion}^0(U^0)\delta(x-x_j) + I(t)\delta(x-x_0) - \sum_{z=1}^{N} P^0\delta(x-x_z), \quad t>0, \tag{19.7}$$

$$C_m V_t^1 = \left(\frac{d_1}{4R_i}\right) V_{xx}^1 - \frac{V^1}{R_{m1}} - \sum_{j=1}^{N} I_{ion}^1(V^1)\delta(x-x_j) - \sum_{j=1}^{\infty} \mathrm{H}[t-(2j-1)\Delta t] I_{syn}^1(V^1) - \sum_{z=1}^{N} P^1\delta(x-x_z), \quad t>0, \tag{19.8}$$

$$C_m V_t^0 = \left(\frac{d_0}{4R_i}\right) V_{xx}^0 - \frac{V^0}{R_{m0}} - \sum_{j=1}^{N} I_{ion}^0(V^0)\delta(x-x_j) - \sum_{j=1}^{\infty} \mathrm{H}[t-2j\Delta t] I_{syn}^0(V^0) - \sum_{z=1}^{N} P^0\delta(x-x_z), \quad t>0, \tag{19.9}$$

where $I_{ion}^i (i=0,1)$ is the current density of various ionic channels embedded in the membrane at $x=x_j$, I (mA/cm) is the input current density of the "0" neuron (only) at $x=x_0$ (see Figure 19.1), and Δt is the axonal delay associated with spike propagation from pre- to postsynaptic neurons (sec). Note that the neurons may have different diameters.

For a network of two chemically coupled neurons, each providing M synaptic inputs to the postsynaptic neurons, the synaptic current is

$$I_{syn}^i(x,t;V^i) = \sum_{k=1}^{M} \delta(x-x_k) g^i(t)[V^i(x,t) - V_{rev}^i], \quad i=0,1, \tag{19.10}$$

where $g^i(t)$ represents the synaptic conductance (S/cm) of the ith neuron at a location governed by the kth synapse from the voltage in the presynaptic neuron whose membrane potential varies with space and time and is usually measured at the soma, and V_{rev}^i is the reversal potential of synaptic receptors on the ith dendritic cable.

Equation (19.10) assumes that all the synapses in the model can be located at arbitrary distances from the cell bodies and can generate conductance changes of different values in the postsynaptic cells due to their varying presynaptic voltages. These assumptions are more realistic than those of previous models. Equation (19.10) accounts for various transmitter-gated ionic currents that are activated at synapses. The voltage of the presynaptic cell is always measured at the soma location (cf. Equations [19.4] and [19.5]), and the dimension of $g^i(t)$ reflects a somewhat unrealistic synaptic knob of infinitesimal width encompassing the entire circumference of the dendrite.

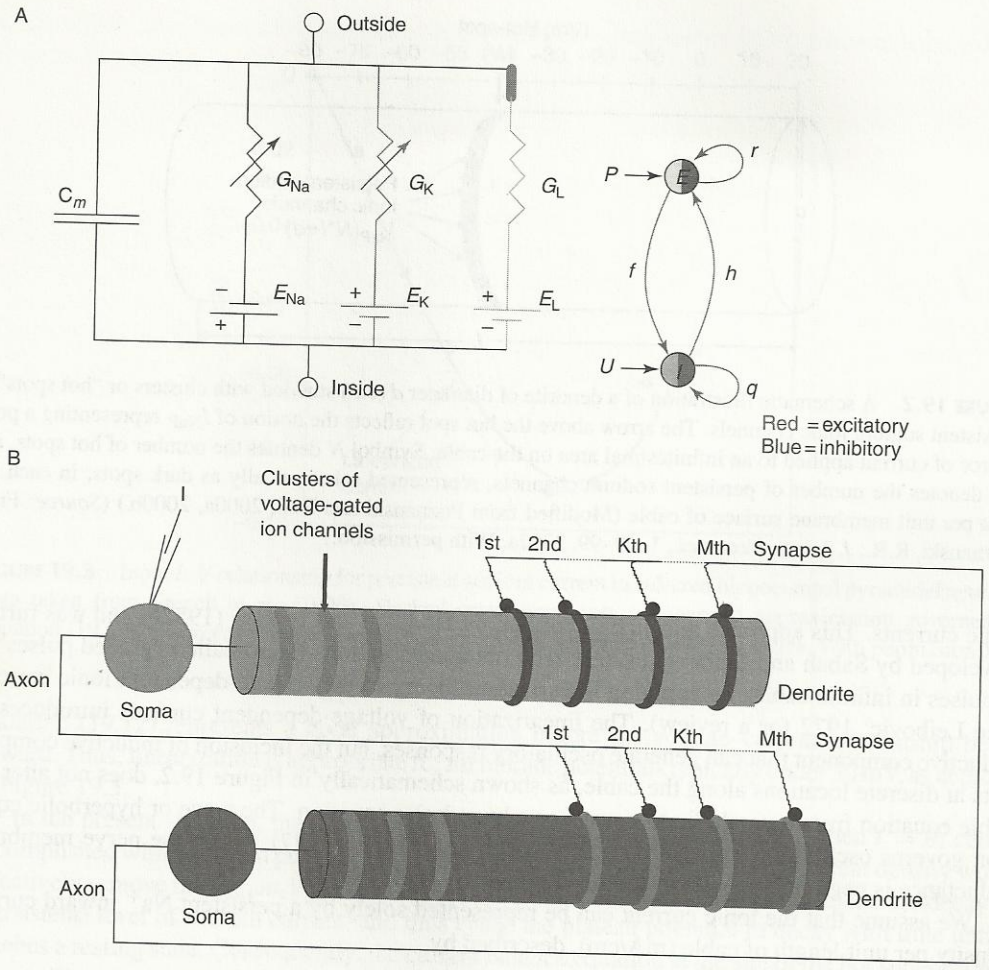

FIGURE 19.1 **(See color insert following page 366)** (A) Schematic illustration of a recurrent network comprising two spiking neurons coupled through synaptic weights. The parameters $\boldsymbol{h}, \boldsymbol{r}, \boldsymbol{f}, \boldsymbol{q}$, represent the strengths of the interactions between the units and $\boldsymbol{P}$, $\boldsymbol{U}$ represent excitatory and inhibitory input respectively. A circuit representation of one conductance-based point neuron is shown. [Kindly provided by Dr. Andrew Gillies, Edinburgh University.] (B) Schematic illustration of a biophysically realistic recurrent network comprising two synaptically coupled neurons. Each neuron is spatially distributed, with a single equivalent ionic cable representing the dendrites and coupled to a lumped isopotential soma. The ionic cable model assumes the cable to be "leaky" (i.e., a passive RC cable) with densities of voltage-dependent ionic channels, referred to as "hot spots," discretely imposed at specific locations along the cable. Nonlinearity is assumed to occur only at these hot spots rather than continuously. The first neuron, "0," is activated by a subthreshold current injection, I, at the soma (represented by the schematic pipette electrode), and the resultant graded electrotonic potential is boosted by persistent Na^+ ionic channels, resulting in neural transmitter release at M axodendritic synapses (chosen at arbitrary locations), which generate synaptic potentials in the second neuron, "1." The same process is repeated from neuron "1" back to neuron "0." (Reproduced from Poznanski, R.R., *J. Integr. Neurosci.*, 1, 69–99, 2002. With permission.)

19.3 Recurrent Dynamics of Two Synaptically Coupled Neurons

19.3.1 Linearization of the Persistent Sodium Current

One way of analytically obtaining the response due to synaptic interactions on ionic cable structures with a finite number of spatially localized ion channels is to linearize the voltage-dependent

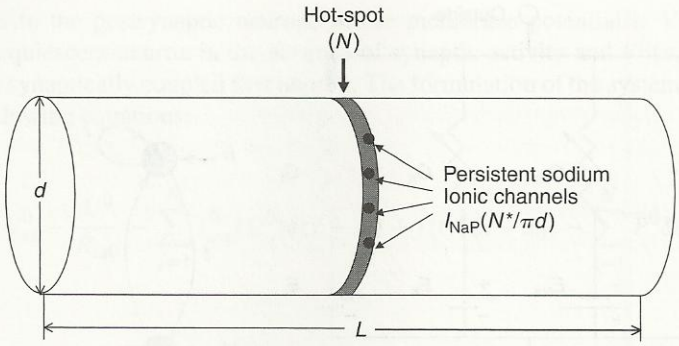

FIGURE 19.2 A schematic illustration of a dendrite of diameter d (cm) studded with clusters or "hot spots" of persistent sodium ionic channels. The arrow above the hot spot reflects the notion of I_{NaP} representing a point source of current applied to an infinitesimal area on the cable. Symbol N denotes the number of hot spots, and N^* denotes the number of persistent sodium channels, represented schematically as dark spots, in each hot spot per unit membrane surface of cable (Modified from Poznanski and Bell, 2000a, 2000b.) (*Source:* From Poznanski, R.R., *J. Integr. Neurosci.*, 1, 69–99, 2002a. With permission.)

ionic currents. This approach was first advocated by Hodgkin and Huxley (1952b) and was further developed by Sabah and Leibovic (1969), who obtained solutions for so-called "graded pulses" or g-pulses in infinite cables by applying linearization theory to the voltage-dependent ionic currents (see Leibovic, 1972 for a review). The linearization of voltage-dependent currents introduces an inductive component that can generate oscillatory responses, but the inclusion of inductive components at discrete locations along the cable, as shown schematically in Figure 19.2, does not alter the cable equation from a parabolic to a wave or a hyperbolic equation. The wave or hyperbolic equation governs oscillatory propagation (cf. Sirovich and Knight, 1977), but in the nerve membrane inductance is negligibly small (see comment made by Rall [1977]).

We assume that the ionic current can be represented solely by a persistent Na^+ inward current density per unit length of cable (mA/cm), described by

$$I^i_{NaP}(x,t;V^i) = g^i_{NaP} m(V^i)[V^i - V^i_{NaP}], \quad i = 0, 1, \tag{19.11}$$

with $V^i_{NaP} = E^i_{NaP} - E_r$, $E_r = -70\,\text{mV}$ is the resting membrane potential, $E^i_{NaP} = 65\,\text{mV}$ is the persistent sodium equilibrium potential (mV), and the strength (conductance) of the persistent sodium ion channel densities is given by (see Hodgkin, 1975) $g^i_{NaP} = g^*_{NaP} N^*$, where $N^*/\pi d_i$ is the number of persistent sodium channels per unit membrane surface of cable in cm^{-1}, and g^*_{NaP} is the maximum attainable conductance of a single sodium channel (=18 pS as measured by Sigworth and Neher [1980] and Stuhmer et al. [1987]). However, other voltage-dependent ionic currents could easily be included in the theory.

Linearization of Equation (19.11) yields

$$I^i_{NaP} = g^i_{NaP} m_r (V^i - V^i_{NaP}) + \tau_{mr} g^i_{NaP} V^i_{NaP} \exp(-t/\tau_{mr}) \times \{m_r[(d\alpha_m/dV^i)_r + (d\beta_m/dV^i)_r] - (d\alpha_m/dV^i)_r\} V^i, \quad i = 0, 1, \quad t > 0, \tag{19.12}$$

where $m_r = \alpha_{mr}/(\alpha_{mr}+\beta_{mr})$, and $\tau_{mr} = 1/(\alpha_{mr}+\beta_{mr})$; α_{mr} and β_{mr} are given by (French et al., 1990):

$$\alpha_{mr} = -1.74(E_r - 11)/\{\exp[-(E_r - 11)/12.94] - 1\}, \tag{19.13}$$

$$\beta_{mr} = 0.06(E_r - 5.9)/\{\exp[(E_r - 5.9)/4.47] - 1\}. \tag{19.14}$$

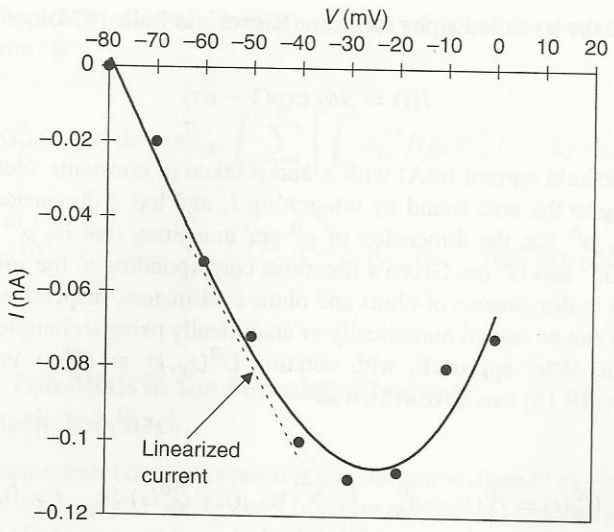

FIGURE 19.3 Input I–V relationship for persistent sodium current in cultured hippocampal pyramidal neurons. Data taken from French et al. (1990). Dashed curve represents a linearized approximation governed by Equation (19.12). (*Source:* From Poznanski, R.R., *J. Integr. Neurosci.*, 1, 69–99, 2002a. With permission.)

Equation (19.12) represents a good approximation before the voltage–current relationship bends upward. Thus, linearization is appropriate for membrane potentials typically under 30 mV, as depicted in Figure 19.3.

In the present situation, the maintenance of zero ionic current at rest (i.e., when $I = 0$) can be accomplished with a sodium pump. The inclusion of an outward sodium-pump current density would effectively remove the $g^i_{\text{NaP}} m_r V^i_{\text{NaP}}$ term in Equation (19.12), which corresponds to the nondecaying (persistent) level of sodium current, and thus cause the plateau potential to decay with time until it reaches a resting state. Consequently, the current balance equation at the site of the hot spot becomes $I^i_{\text{NaP}} + P^i = 0$, where $P^i = g^i_{\text{NaP}} m_r V^i_{\text{NaP}}$ is the outward sodium-pump current density.

19.3.2 Electrotonic Potential in the Stimulated Neuron

If the outward sodium-pump current density is positive (by convention), then $P^0 = g_{\text{NaP}} m_r V^o_{\text{NaP}}$. If we assume that the hot-spot points "i" and sodium-pump points "z" are juxtaposed on the cable, and take advantage of linearity and use Green's function methods to solve Equation (19.7) (see Tuckwell, 1988a, p. 191), we can readily obtain a Neumann–Volterra series expansion for the voltage in response to a current injection at the soma in the presence of persistent sodium ion channels at localized points on the cable:

$$U^0(x,t) = \int_0^t \left[I(s) G^{*0}(x,0;t-s) - g^0_{\text{NaP}} \sum_{j=1}^{N} \rho^{u0}(s) U^0(x_j,s) G^0(x,x_j;t-s) \right] \mathrm{d}s, \quad t > 0, \tag{19.15}$$

where

$$\rho^{u0}(t) = m_r - \tau_{mr} V^0_{\text{NaP}} \{ (\mathrm{d}\alpha_m/\mathrm{d}U^0)_r - m_r [(\mathrm{d}\alpha_m/\mathrm{d}U^0)_r + (\mathrm{d}\beta_m/\mathrm{d}U^0)_r] \} \exp(-t/\tau_{mr})$$

is dimensionless, and the so-called alpha function (Rinzel and Rall, 1974):

$$I(t) = \beta\alpha t \exp(1 - \alpha t)$$

is the applied subthreshold current (mA) with α and β taken as constants. Note that β' is the input charge corresponding to the area found by integrating I, and has a dimension of β per unit time, that is, $\beta' = \beta/\text{sec}$, $\rho^{0\prime}$ has the dimension of ρ^0 per unit time, that is, $\rho^{0\prime} = \rho^0/\text{sec}$ found by integrating ρ^0, and G^{*0} and G^0 are Green's functions corresponding to the solution of the standard linear cable equation in dimensions of ohms and ohms centimeters, respectively (see Appendix).

Equation (19.15) can be solved numerically or analytically using techniques found in Poznanski (1990). Adopting this latter approach, with notation $U^0(x_p, t) \equiv U_p^0(t)$ and $G(x_p, x_0, t - s) \equiv G_{p0}(t - s)$, Equation (19.15) can be rewritten as

$$U_p^0(t) = f_p^0(t) - g_{\text{NaP}}^0 \int_0^t \sum_{j=1}^{N} \aleph_{0pj}(t, s) U_j^0(s)\, \mathrm{d}s, \quad t > 0, \tag{19.16}$$

where

$$f_p^0(t) = \int_0^t \lambda_0^{-1} I(s) G_{p0}^0(t - s)\, \mathrm{d}s \quad \text{and} \quad \aleph_{0pj}(t, s) = G_{pj}^0(t - s)\rho^{u0}(s).$$

The system of Volterra integral equations becomes amenable to the following analytical solution corresponding to the voltage response at $x = x_p$ in response to a current injection at $x = 0$, and hot spots at $x = x_j$:

$$U_p^0(t) = f_p^0(t) - g_{\text{NaP}}^0 \int_0^t \sum_{j=1}^{N} \Re_{pj}(t, s) f_j^0(s)\, \mathrm{d}s, \quad t > 0, \tag{19.17}$$

where the kernels, $\Re_{pj}$, are the sums of the uniformly convergent series

$$\Re_{pj}(t, s) = \aleph_{0pj}(t, s) + \sum_{\nu=1}^{\infty} (g_{\text{NaP}}^0)^\nu (-1)^\nu \aleph_{0pj}^{(\nu)}(t, s) \tag{19.18}$$

and the ν-fold iterated kernels, $\aleph_{0pj}^{(\nu)}$, are defined inductively by the relation

$$\begin{aligned} \aleph_{0pj}^{(\nu)}(t, s) &= \sum_{\gamma=1}^{N} \int_s^t \aleph_{0p\gamma}(t, \xi) \aleph_{0\gamma j}^{(\nu-1)}(\xi, s)\, \mathrm{d}\xi \\ &= \sum_{\gamma=1}^{N} \int_s^t \aleph_{0p\gamma}(t, \xi_1) \aleph_{0\gamma j}(\xi_1, s) \prod_{h=2}^{\nu} \left\{ \int_s^{\xi_{h-1}} \aleph_{0p\gamma}(\xi_{h-1}, \xi_h)\, \mathrm{d}\xi_h \right\} \mathrm{d}\xi_1 \end{aligned} \tag{19.19}$$

with

$$\aleph_{0\gamma j}^{(0)} \equiv \aleph_{0\gamma j} \quad \text{and} \quad \aleph_{0pj}^{(1)}(t, s) = \sum_{\gamma=1}^{N} \int_s^t \aleph_{0p\gamma}(t, \xi_1) \aleph_{0\gamma j}(\xi_1, s)\, \mathrm{d}\xi_1.$$

Finally, after some simplification, the following solution is obtained for the electrotonic potential in current-injected neuron "0":

$$U_p^0(t) \approx \int_0^t \lambda_0^{-1} I(s) G_{p0}^0(t-s)\,\mathrm{d}s - g_{\mathrm{NaP}}^0 \int_0^t \sum_{j=1}^{N} \left\{ \int_0^s \lambda_0^{-1} I(\xi_0) G_{j0}^0(s-\xi_0)\,\mathrm{d}\xi_0 \right\}$$
$$\times \left[G_{pj}^0(t-s)\rho^0(s) - g_{\mathrm{NaP}}^0 \sum_{\gamma=1}^{N} \int_s^t G_{p\gamma}^0(t-\xi_1) G_{\gamma j}^0(\xi_1 - s)\rho^{u0}(s)\rho^{u0}(\xi_1)\,\mathrm{d}\xi_1 \right] \mathrm{d}s, \quad t > 0. \tag{19.20}$$

19.3.3 Dendritic Potentials in the Stimulated Neuron with Synaptic Feedback

If outward sodium-pump current density is positive by convention, then $P^i = g_{\mathrm{NaP}}^i m_{\mathrm{r}} V_{\mathrm{NaP}}^i$. By taking advantage of linearity and applying the Green's function method of solution (see Tuckwell, 1988b, p. 191) to Equations (19.8) and (19.9), a Volterra series expansion for the voltage in response to synaptic inputs treated as conductance changes impinging at localized points on the cable with localized synaptic conductance changes for specific ions can be readily obtained by linearizing Equation (19.10), that is, $V^i(x_k, t) \ll V_{\mathrm{rev}}^i$, which is a valid approximation when considering the NMDA and AMPA receptor channels. The linearization of synaptic current has been taken into consideration by Amit and Tsodyks (1992), Tuckwell et al. (1996), and Chapeau-Blondeau and Chambert (1995).

Let the membrane potential of the neuron activated by a current injection to the soma be $V^0(x,t)$ and the membrane potential of the synaptically coupled neuron as $V^1(x,t)$. As the first neuron has synaptic feedback from the coupled neuron a similar expression to that for the electrotonic potential can be obtained for the synaptically coupled neurons, as depicted in Figure 19.1, viz.

$$V^0(x,t) = U^0(x,t) - \int_0^t \left[\sum_{y=1}^{\infty} \mathrm{H}[s - 2y\Delta t] \sum_{k=1}^{M} g^0(s) V_{\mathrm{rev}}^0 G^0(x, x_k; t-s) \right.$$
$$\left. + g_{\mathrm{NaP}}^0 \sum_{j=1}^{N} \rho^{v0}(s) V^0(x_j, s) G^0(x, x_j; t-s) \right] \mathrm{d}s, \quad t > 0, \tag{19.21}$$

where

$$\rho^{v0}(t) = m_{\mathrm{r}} - \tau_{mr} V_{\mathrm{NaP}}^0 \{(\mathrm{d}\alpha_m/\mathrm{d}V^0)_{\mathrm{r}} - m_{\mathrm{r}}[(\mathrm{d}\alpha_m/\mathrm{d}V^0)_{\mathrm{r}} + (\mathrm{d}\beta_m/\mathrm{d}V^0)_{\mathrm{r}}]\} \exp(-t/\tau_{mr})$$

and $g^{0\prime}$ has the dimension of g^0 per unit time, that is, $g^{0\prime} = g^0/\mathrm{sec}$ found from integrating g^0.

The system of Volterra integral equations governed by Equation (19.21) may be rewritten as

$$V_p^0(t) = f_p^0(t) - g_{\mathrm{NaP}}^0 \int_0^t \sum_{j=1}^{N} \aleph_{1pj}(t,s) V_j^0(s)\,\mathrm{d}s, \quad t > 0, \tag{19.22}$$

where

$$f_p^0(t) = U_p^0(t) - V_{\mathrm{rev}}^0 \int_0^t \sum_{y=1}^{\infty} \mathrm{H}[s - 2y\Delta t] \sum_{k=1}^{M} g^0(s) G_{pk}^0(t-s)\,\mathrm{d}s$$

and $\aleph_{1pj}(t,s) = G^0_{pj}(t-s)\rho^{\nu 0}(s)$. The above system of Volterra integral equations is amenable to the following analytical solution corresponding to the voltage response at $x = x_p$ in response to current injection at the soma, a composite synaptic input at location $x = x_k$, and hot spots at $x = x_j$:

$$V^0_p(t) = f^0_p(t) - g^0_{\mathrm{NaP}} \int_0^t \sum_{j=1}^{N} \Re_{pj}(t,s) f^0_j(s)\, \mathrm{d}s, \quad t > 0, \tag{19.23}$$

where the resolvent kernels, $\Re_{pj}$, are the sums of the uniformly convergent series given by Equation (19.18) with $\aleph_0$ replaced by $\aleph_i$, and the ν-fold iterated kernels, $\aleph^{(\nu)}_{1pj}$, are defined inductively by the relation given by Equation (19.19) with $\aleph_0$ replaced with $\aleph_1$. After some simplification, the following solution is obtained for the synaptic potentials:

$$\begin{aligned} V^0_p(t) \approx U^0_p(t) - V^0_{\mathrm{rev}} \int_0^t \sum_{y=1}^{\infty} \mathrm{H}[s - 2y\Delta t] \sum_{k=1}^{M} g^0(s) G^0_{pk}(t-s)\, \mathrm{d}s \\ - g^0_{\mathrm{NaP}} \int_0^t \left(\sum_{j=1}^{N} \left\{ U^0_p(s) - V^0_{\mathrm{rev}} \int_0^s \sum_{y=1}^{\infty} \mathrm{H}[\xi_0 - 2y\Delta t] \right.\right. \\ \left. \times \sum_{k=1}^{M} g^0(\xi_0) G^0_{jk}(s-\xi_0)\, \mathrm{d}\xi_0 \right\} \\ \times \left[G^0_{pj}(t-s)\rho^{\nu 0}(s) - g^0_{\mathrm{NaP}} \sum_{\gamma=1}^{N} \int_s^t G^0_{p\gamma}(t-\xi_1) G^0_{\gamma j}(\xi_1 - s)\rho^{\nu 0}(s) \right. \\ \left.\left. \times \rho^{\nu 0}(\xi_1)\, \mathrm{d}\xi_1 \right] \right) \mathrm{d}s, \quad t > 0. \end{aligned} \tag{19.24}$$

The conductance change $g^0(t)$ at the kth synapse on the stimulated neuron emanating from the coupled neuron was found by solving Equation (19.6) subject to initial condition $g(2y\Delta t) = 0$ (Chapeau-Blondeau and Chambert, 1995):

$$\begin{aligned} g^0(t) = (g^0_{\mathrm{sat}}\omega/\tau_g) \int_{2y\Delta t}^{t} C^0(t'') \exp\left[\frac{t'' - 2y\Delta t}{\tau_g} + \left(\frac{\omega}{\tau_g}\right) \int_{2y\Delta t}^{t''} C^0(t')\, \mathrm{d}t' \right] \mathrm{d}t'' \\ \times \exp\left[\frac{t - 2y\Delta t}{\tau_g} - \left(\frac{\omega}{\tau_g}\right) \int_{2y\Delta t}^{t} C^0(t')\, \mathrm{d}t' \right], \end{aligned} \tag{19.25}$$

where $C^{0\prime}$ has the dimension of C^0 per unit time, that is, $C^{0\prime} = C^0/\mathrm{sec}$ found by integrating C^0. The concentration of neural transmitter in the synaptic cleft, as a result of spiking activity at the kth synapse on the stimulated neuron emanating from the coupled neuron, was found by substituting Equation (19.4) into Equation (19.5) with initial condition $C^0(2y\Delta t) = C_0$ to yield:

$$C^0(t) = C_0 \exp\left[-\left(\frac{t - 2y\Delta t}{\tau_c} \right) \right] \sum_{k=1}^{N_{\mathrm{sp}}} \mathrm{H}[V^1(t_k + (2y-1)\Delta t) - \theta], \tag{19.26}$$

where t_k is measured from $t = (2y-1)\Delta t$, with $y = 1, 2, \ldots$.

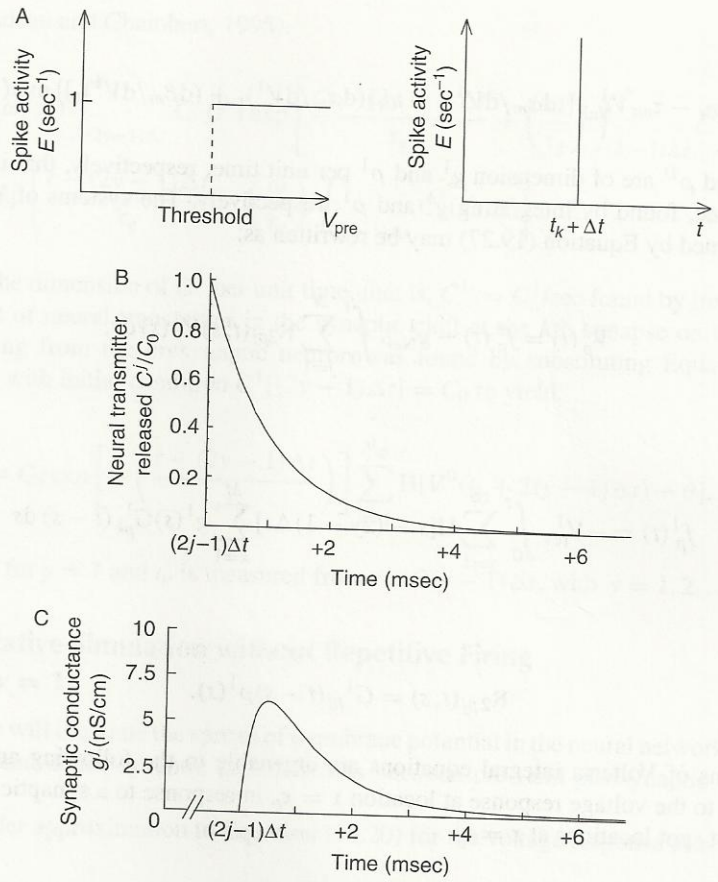

FIGURE 19.4 (A) Spike-train activity is recorded at the synapse every t_k sec if the presynaptic voltage (at a point near the fictitious soma or axon hillock) is above threshold, measured at time intervals of $t_k + \Delta t$ where Δt is the axonal delay. (B) The concentration of neural transmitter in the synaptic cleft as a function of time. (C) The conductance change (nS/cm) resulting at each synapse as a function of time. See Table 19.1 for parameter values used. (*Source*: From Poznanski, R.R., *J. Integr. Neurosci.*, 1, 69–99, 2002a. With permission.)

Figure 19.4 shows typical concentrations of a neural transmitter in the synaptic clefts of all synapses with a slightly more rapid decay for the synapses presynaptic to the second neuron, and the conductance change as a result of the neural transmitter attaching to the receptors in the postsynaptic membrane.

19.3.4 Dendritic Potentials in the Nonstimulated Neuron via Feedforward Synapses

A similar expression results for the second synaptically coupled neuron as outlined in Section 19.3.3:

$$V^1(x,t) = -\int_0^t \sum_{y=1}^{\infty} \mathrm{H}[s-(2y-1)\Delta t]\left[\sum_{k=1}^{M} g^1(s)V^1_{\mathrm{rev}}G^1(x,x_k;t-s)\right.$$

$$\left. + g^1_{\mathrm{NaP}} \sum_{j=1}^{N} \rho^1(s)V^1(x_j,s)G^1(x,x_j;t-s)\right] \mathrm{d}s, \qquad (19.27)$$

where

$$\rho^1(t) = m_r - \tau_{mr} V^1_{NaP}\{(d\alpha_m/dV^1)_r - m_r[(d\alpha_m/dV^1)_r + (d\beta_m/dV^1)_r]\}\exp(-t/\tau_{mr}).$$

Note that $g^{1\prime}$ and $\rho^{1\prime}$ are of dimension g^1 and ρ^1 per unit time, respectively, that is, $g^{1\prime} = g^1/\text{sec}$ and $\rho^{1\prime} = \rho^1/\text{sec}$, found by integrating g^1 and ρ^1, respectively. The systems of Volterra integral equations governed by Equation (19.27) may be rewritten as:

$$V^1_p(t) = f^1_p(t) - g^1_{NaP}\int_0^t \sum_{j=1}^{N} \aleph_{2pj}(t,s)V^1_j(s)\,ds, \tag{19.28}$$

where

$$f^1_p(t) = -V^1_{rev}\int_0^t \sum_{y=1}^{\infty} H[s-(2y-1)\Delta t]\sum_{k=1}^{M} g^1(s)G^1_{pk}(t-s)\,ds$$

and

$$\aleph_{2pj}(t,s) = G^1{}_{pj}(t-s)\rho^1(s).$$

The systems of Volterra integral equations are amenable to the following analytical solution corresponding to the voltage response at location $x = x_p$ in response to a synaptic input at location $x = x_k$, and hot spot locations at $x = x_j$

$$V^1_p(t) = f^1_p(t) - g^1_{NaP}\int_0^t \sum_{j=1}^{N} \Re_{pj}(t,s)f^1_j(s)\,ds, \quad t > 0. \tag{19.29}$$

where the resolvent kernels, $\Re_{pj}$, are the sums of the uniformly convergent series given by Equation (19.18) with $\aleph_0$ replaced by $\aleph_2$, and the ν-fold iterated kernels $\aleph^{(\mu)}_{2pj}$ are defined inductively by the relation given by Equation (19.19) with $\aleph_0$ replaced with $\aleph_2$. After some simplification the following solution is obtained for the synaptic potentials:

$$\begin{aligned} V^1_p(t) \approx V^1_{rev}\Bigg(&- \int_0^t \sum_{y=1}^{\infty} H[s-(2y-1)\Delta t]\sum_{k=1}^{M} g^1(s)G^1_{pk}(t-s)\,ds \\ &+ g^1_{NaP}\int_0^t \sum_{j=1}^{N}\left\{\int_0^s \sum_{y=1}^{\infty} H[\xi_0-(2y-1)\Delta t]\sum_{k=1}^{M} g^1(\xi_0)G^1_{jk}(s-\xi_0)\,d\xi_0\right\} \\ &\times\Bigg[G^1_{pj}(t-s)\rho^1(s) + g^1_{NaP}\sum_{\gamma=1}^{N}\int_s^t G^1_{p\gamma}(t-\xi_1) \\ &\times G^1_{\gamma j}(\xi_1-s)\rho^1(s)\rho^1(\xi_1)\,d\xi_1\Bigg]\,ds\Bigg), \quad t > 0. \end{aligned} \tag{19.30}$$

Conductance change $g^1(t)$ at the kth synapse on the postsynaptic neuron emanating from the presynaptic neuron was found by solving Equation (19.6) subject to initial condition $g[(2y-1)\Delta t] = 0$

(Chapeau-Blondeau and Chambert, 1995):

$$g^1(t) = (g^1_{\text{sat}}\omega/\tau_g)\int_{(2y-1)\Delta t}^{t} C^1(t'')\exp\left[\frac{t''-(2y-1)\Delta t}{\tau_g} + \left(\frac{\omega}{\tau_g}\right)\int_{(2y-1)\Delta t}^{t''} C^1(t')\,dt'\right]dt''$$
$$\times \exp\left[\frac{t-(2y-1)\Delta t}{\tau_g} - \left(\frac{\omega}{\tau_g}\right)\int_{(2y-1)\Delta t}^{t} C^1(t')\,dt'\right], \tag{19.31}$$

where $C^{1\prime}$ has the dimension of C^1 per unit time, that is, $C^{1\prime} = C^1/\text{sec}$ found by integrating C^1.

The amount of neural transmitter in the synaptic cleft at the kth synapse on the postsynaptic neuron emanating from the presynaptic neuron was found by substituting Equation (19.4) into Equation (19.5) with initial condition $C^1[(2y-1)\Delta t] = C_0$ to yield:

$$C^1(t) = C_0\exp\left[-\left(\frac{t-(2y-1)\Delta t}{\tau_c}\right)\right]\sum_{k=1}^{N_{\text{sp}}} \text{H}[V^0(t_k + 2(y-1)\Delta t) - \theta], \tag{19.32}$$

where $U^0 \equiv V^0$ for $y = 1$ and t_k is measured from $t = 2(y-1)\Delta t$, with $y = 1, 2, \ldots$.

19.3.5 Illustrative Simulation without Repetitive Firing (i.e., $y = 1$)

In this section we will illustrate the spread of membrane potential in the neural network of Figure 19.1 for both sparse and dense synaptic connectivities between pre- and postsynaptic neurons in the network.

A second-order approximation to Equation (19.20) for the voltage response at $x = x_p$ is

$$U^0_p(t) \approx \int_0^t \lambda_0^{-1} I(s) G^0_{p0}(t-s)\,ds - g_{\text{NaP}}\int_0^t \left\{\sum_{j=1}^{N} \rho^{u0}(s) G^0_{pj}(t-s)\int_0^s \lambda_0^{-1} I(\xi_0) G^0_{j0}(s-\xi_0)\,d\xi_0\right\}. \tag{19.33}$$

A second-order approximation to Equation (19.24) for the voltage response at $x = x_p$ with $y = 1$ is

$$V^0_p(t) \approx U^0_p(t) - V^0_{\text{rev}}\int_{2\Delta t}^{t}\sum_{k=1}^{M} g^0(s) G^0_{pk}(t-s)\,ds$$
$$+ g^0_{\text{NaP}}\int_{2\Delta t}^{t}\sum_{j=1}^{N} G^0_{pj}(t-s)\rho^{v0}(s)\int_{2\Delta t}^{s} V^0_{\text{rev}}\sum_{k=1}^{M} g^0(\xi_0) G^0_{jk}(s-\xi_0)\,d\xi_0\,ds$$
$$- g^0_{\text{NaP}}\int_0^t\sum_{j=1}^{N}\rho^{v0}(s) G^0_{pj}(t-s) U^0_p(s)\,ds, \quad t > 0, \tag{19.34}$$

where

$$g^0(t) = (g^0_{\text{sat}}\omega/\tau_g)\int_{2\Delta t}^{t} C^0(t'')\exp\left[\frac{t''-2\Delta t}{\tau_g} + \left(\frac{\omega}{\tau_g}\right)\int_{2\Delta t}^{t''} C^0(t')\,dt'\right]dt''$$
$$\times \exp\left[\frac{t-2\Delta t}{\tau_g} - \left(\frac{\omega}{\tau_g}\right)\int_{2\Delta t}^{t} C^0(t')\,dt'\right] \tag{19.35}$$

and

$$C^0(t) = C_0 \exp\left[-\left(\frac{t-2\Delta t}{\tau_c}\right)\right] \sum_{k=1}^{N_{sp}} \mathrm{H}[V^1(t_k + \Delta t) - \theta]. \tag{19.36}$$

A second-order approximation to Equation (19.30) with $y = 1$ is

$$\begin{aligned} V_p^1(t) \approx & V_{rev}^1 \Bigg(- \int_{\Delta t}^{t} \sum_{k=1}^{M} g^1(s) G_{pk}^1(t-s)\, \mathrm{d}s \\ & + g_{NaP}^1 \int_{\Delta t}^{t} \left\{ \sum_{j=1}^{N} \rho^1(s) G_{pj}^1(t-s) \int_{\Delta t}^{s} \sum_{k=1}^{M} G_{jk}^1(s-\xi_0) g^1(\xi_0)\, \mathrm{d}\xi_0 \right\} \mathrm{d}s \Bigg), \\ & t > \Delta t, \end{aligned} \tag{19.37}$$

where

$$\begin{aligned} g^1(t) = & (g_{sat}^1 \omega/\tau_g) \int_{\Delta t}^{t} C^1(t'') \exp\left[\frac{t''-\Delta t}{\tau_g} + \left(\frac{\omega}{\tau_g}\right) \int_{\Delta t}^{t''} C^1(t')\, \mathrm{d}t'\right] \mathrm{d}t'' \\ & \times \exp\left[\frac{t-\Delta t}{\tau_g} - \left(\frac{\omega}{\tau_g}\right) \int_{\Delta t}^{t} C^1(t')\, \mathrm{d}t'\right] \end{aligned} \tag{19.38}$$

and

$$C^1(t) = C_0 \exp\left[-\left(\frac{t-\Delta t}{\tau_c}\right)\right] \sum_{k=1}^{N_{sp}} H[U^0(t_k) - \theta]. \tag{19.39}$$

Equations (19.33), (19.34), and (19.37) were evaluated using the *Mathematica*™ (Version 3.0) software. The computation required under 60 min on a HITACHI Flora™ 370 workstation with a 400 MHz CPU and 384 MB memory provided the first three terms in the Green's function are used. The first term of the Green's function dominates; the other terms decrease exponentially with time, therefore no significant difference in results occurred by truncating the Green's function. However, at small times ($t < 0.01$) an alternative Green's function should be used that converges more rapidly (see Section 19.3.5). Simulations were done using the parameter values given in Table 19.1 for a nonuniform distribution of hot spots and in the presence of no hot spots (Figure 19.5 and Figure 19.6).

In Figure 19.5 we have illustrated the passive and weakly regenerative backpropagation of electrotonic potential in neuron "0" as a consequence of stimulating the soma by current injection and without synaptic feedback from neuron "1." It is clear that the backpropagating potential falls in amplitude below threshold (i.e., under 10 mV). The distribution of voltage-dependent ion channels in close proximity to the soma yields only a minor increase in the peak amplitude as measured at the terminal end of the cable, suggesting that the axosomatic distribution of voltage-dependent ion channels plays a minor role in dendritic integration.

In Figure 19.6 we have illustrated the formation of dendritic spike-like potentials or excitatory postsynaptic-like potentials (EPSLPs) at a distally placed location along the dendrite of stimulated neuron "0" as a consequence of synaptic feedback from neuron "1" and both passive and weakly regenerative backpropagation of electrotonic potentials. Some important results that have

TABLE 19.1
Parameters for Synaptic Transmission

Parameter	Value	Reference
θ	7–15 mV	Hodgkin and Huxley (1952b)
Δt	6 msec	Kawaguchi and Fukunishi (1998)
τ_k	20 msec	Kawaguchi and Fukunishi (1998)
τ_c	1 msec	Kurogi (1987)
τ_g	1 msec	Chapeau-Blondeau and Chambert (1995)
ω	2 mM^{-1}	Chapeau-Blondeau and Chambert (1995)
C_0	1 mM	Chapeau-Blondeau and Chambert (1995)
g_{max}	20 pS	Hille (2001)
M^*	10–1000	Korn and Faber (1991)
V^i_{rev}	100 mV	Tuckwell et al. (1996)
g^0_{sat}	25.46 μS/cm	Based on $d_0 = 2.5$ μm and $M^* = 1000$
g^1_{sat}	17.2 μS/cm	Based on $d_1 = 3.7$ μm and $M^* = 1000$
N_{sp}	1	A single spike activates transmitter

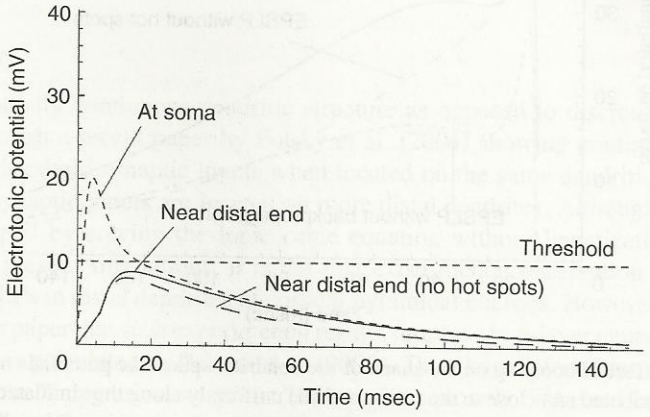

FIGURE 19.5 Electrotonic potentials in neuron "0" measured at $x_p = 0.0$ (dotted line) and $x_p = 0.9L$ (solid line) along the dendritic cable in the presence of persistent sodium ionic channels and at $x_p = 0.9L$ (dashed line) in the absence of persistent sodium hot spots. A current step of magnitude I_0 is injected at the soma (i.e., at $x_p = 0$) with the resultant amplification of electrotonic potentials mediated by $N = 16$ persistent sodium hot spots distributed close to the soma with a constant density of $N^* = 10$. The key parameters were $R_a = 200\,\Omega$ cm, $R_{m0} = 40{,}000\,\Omega\,cm^2$, $L_0 = 800\,\mu$m, $d_0 = 2.5\,\mu$m, $\lambda_0 = 0.1118$ cm, $g^0_{NaP} = 0.229\,\mu$S/cm, $\beta = 0.3$ mA, and $\alpha = 0.25$/msec. The values of β and α were selected arbitrarily to yield a response at the soma of approximately 9.0 mV in the absence of persistent sodium hot spots. (*Source:* From Poznanski, R.R., *J. Integr. Neurosci.*, 1, 69–99, 2002a. With permission.)

been observed experimentally clearly indicate the data shown in Figure 19.6. In Figure 19.6A it can be seen that, unlike the results presented in Figure 19.5 where the distal electrotonic potential falls below threshold, the peak amplitude of the synaptic potential as a result of feedback from neuron "1" is well above threshold and produces a "dendritic spike." The effect of back-propagation is to further amplify the dendritic spike from about 28 to 37 mV. As is the case with the data shown in Figure 19.5, the results in Figure 19.6A reveal that hot spots concentrated in close proximity to the soma are of negligible consequence for the membrane potential recorded at the distal tip of neuron "0." However, in Figure 19.6B the voltage-dependent ionic channels are

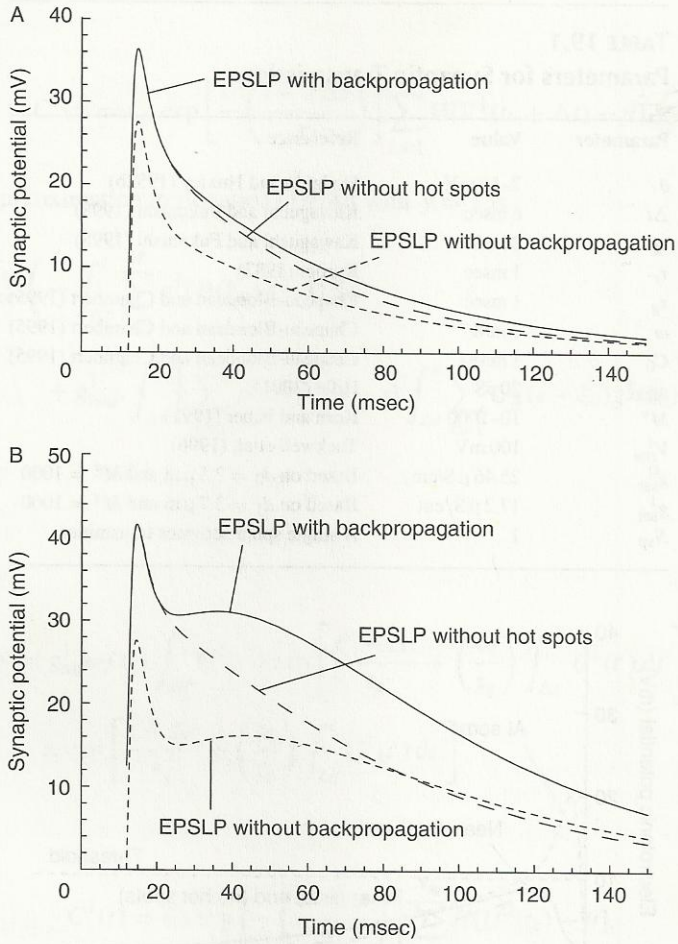

FIGURE 19.6 The effect of boosting on the shape of the dendritic spike-like potentials mediated by persistent sodium hot spots distributed (A) close to the soma, and (B) uniformly along the simulated neuron as a result of synaptic feedback from the nonstimulated neuron "0" with inputs distributed peripherally along the dendritic cable of the stimulated neuron ($M = 24$). The curves are for dendritic spikes at $x_p = 0.9L$ (solid line) and without hot spots (dashed line), and without backpropagating electrotonic potentials (dotted line) for a subthreshold current input at $x_0 = 0$ (soma). The key parameters were $R_a = 200\,\Omega\,\text{cm}$, $R_{m0} = 40{,}000\,\Omega\,\text{cm}^2$, $R_{m1} = 50{,}000\,\Omega\,\text{cm}^2$, $L_0 = 800\,\mu\text{m}$, $L_1 = 1{,}000\,\mu\text{m}$, $d_0 = 2.5\,\mu\text{m}$, $d_1 = 3.7\,\mu\text{m}$, $\lambda_0 = 0.1118\,\text{cm}$, $\lambda_1 = 0.152\,\text{cm}$, $g^0_{NaP} = 0.229\,\mu\text{S/cm}$, $g^1_{NaP} = 0.155\,\mu\text{S/cm}$, $\beta = 0.3\,\text{mA}$, and $\alpha = 0.25/\text{msec}$. The values of β and α were selected arbitrarily to yield a response at the soma of approximately 9.0 mV in the absence of sodium persistent hot spots. (*Source:* From Poznanski, R.R., *J. Integr. Neurosci.*, 1, 69–99, 2002a. With permission.)

distributed uniformly throughout the dendritic cable of neuron "0" and neuron "1." The results in this case reveal a further amplification in the peak amplitude of the dendritic spike in comparison with the synaptic potentials seen in Figure 19.6A. In particular, the effect of spatially distributing the persistent sodium channels is to boost the peak amplitude of the dendritic spike to about 42 mV (Figure 19.6B), in comparison to about 37 mV when the persistent sodium channels are located proximal to the soma (Figure 19.6A). It is particularly interesting that the peak amplitude of the synaptic potential measured at the distal end of neuron "0" is left relatively unchanged by changes in the spatial distribution of persistent sodium channels in the case when backpropagation of the signal is not taken into consideration. As shown in both Figure 19.6A and Figure 19.6B the peak

amplitude of the dendritic spike remains constant at 28 mV. This result suggests that the spatially distributed voltage-dependent ion channels boost the peak amplitude of the dendritic spikes during their propagation. Another important result that can be seen by comparing the results in Figure 19.6A and Figure 19.6B is that the peak amplitude of the EPSLP without hot spots reaches about 42 mV in Figure 19.6B but only 37 mV for the same EPSLP in Figure 19.6A. What causes this discrepancy in peak amplitude when the only difference in the models generating the results in the two figures is the spatial distribution of voltage-dependent ionic channels? The answer is that the synaptic input driving the EPSLP in Figure 19.6B is marginally stronger than that driving the EPSLP in Figure 19.6A. In other words, the presynaptic voltage drives the kinetics of the synaptic conductance in the postsynaptic neuron. Such effects on synaptic potentiation as a result of network properties is a testament to the power of biophysically realistic neural networks, such as the ones presented here, and suggests that such networks may be useful for the investigation of associative learning principles.

A final observation that is also evident by comparing Figure 19.6A with Figure 19.6B is the fact that the spatial distribution of ionic channels produces a broadening in the time course of the EPSLP both with and without backpropagation. Such broadening is of course absent in EPSLPs without hot spots (dashed line in Figure 19.6B). The broadening in the time course of the dendritic spikes may also play a role in dendritic integration and associative learning.

19.4 Discussion

The need for a spatially continuous dendritic structure as opposed to discretized caricatures can be exemplified through a recent paper by Polsky et al. (2004) showing nonlinear (or superlinear) summation of subthreshold synaptic inputs when located on the same dendritic branch, but linear summation when synaptic inputs are located on more distal dendrites. Although these conclusions can be easily grasped by solving the ionic cable equation without linearization of the synaptic current as used in present simulations, it is the first experimental observation showing nonlinear summation of EPSLPs in distal dendrites of cortical pyramidal neurons. However, the authors argue haphazardly in their paper that such experimental results support a two-layer neural network model of pyramidal neurons as postulated by Poirazi et al. (2003). This claim is fortuitous as it gives pretense to the existence of the "integration zones" or "subunits" commonly discussed in the computational neuroscience literature. Experimental evidence provided by Polsky et al. (2004) does not support the notion of single neurons having any segregating mechanisms allowing for compartmentalization of dendrites to form computational subunits, but simply advocates the importance of the spatial distribution of synaptic inputs in dendritic integration, which is impossible to examine with point neuron models. In order to circumvent stringent criteria for generating computational subunits in dendrites of cortical pyramidal neurons corresponding to a one-to-one mapping between dendrite and subunit, Polsky et al. (2004) advocate a less stringent notion of "sliding window" or "sliding" subunits of less than 100 μm as a basic integrative compartment. However, the experimental results of Polsky et al. (2004) pertaining to a "sliding" subunit are not functionally equivalent to a two-layer model as suggested by Spruston and Kath (2004). Two-layer models assume a rigid subunit structure with a clearly defined "integration zone," yet in the Polsky et al. (2004) paper a more fluid conception with a "sliding" subunit organization is advocated. The latter can be modeled only when spatially continuous dendrites with hot spots of synaptic activity manifest into an artificially transient or "sliding" subunit aurora in the membrane potential. This differs drastically from the rigid "computational" subunits explored in two-layer models, yet is compatible with the methodology pioneered by Poznanski (2002a).

Recently, Izhikevich et al. (2004) have presented a neuronal network model based on an elaborated kind of integrate-and-fire "point" neuron that incorporates receptor kinetics, axonal delays, and short-term as well as spike-timing-dependent long-term synaptic plasticity. Although such an

approach is convenient for large-scale simulations of neuronal networks while going well beyond the level of detail in other integrate-and-fire neuron models, it still does not capture the fine detail possible with biophysically realistic continuous-membrane neuronal models. Here are some essential characteristics which we consider that biological networks should possess to be dynamically suited to model the processing of neural information:

- The network has the capacity for adaptability.
- Firing rate or transfer function at the axon hillock is dependent on ionic channels that are modulated by various neurotransmitters, neuromodulators, and second messengers.
- Synaptic weights pertaining to synaptic efficacy of the networks are chemically tuned.
- Functional connectivity is dynamic, that is, changes "fluidly."

The above characteristics can be interpreted as being essential for modeling biophysically realistic neural networks. To obtain them, ionic channels should be included at discrete locations and synaptic weights should be replaced with a conductance changes occurring on the postsynaptic neurons. The notion of "fluidity" of connectivity can be mimicked with the introduction of spatial dimensionality and the movement of synaptic connections along the neuronal structure in response to appropriate electric and chemical signals. Neuromorphic models of networks with each neuron represented by a reduced ionic cable provide three hierarchic levels (subcellular, cellular, and network) of neural organization. Such multilevel models should reproduce neurophysiologic data involving spatiotemporal processing with greater dynamical and functional prowess.

Biophysical mechanisms governing signal processing at the individual neuron level do not succeed in explaining brain function, yet coupled with a view of the brain as a collection of interacting distributed systems of biophysical neural networks; a more powerful approach to the understanding of brain function is possible. Research on how brain function arises from biophysical mechanisms modeled at the neural network level is vital to understanding brain function from an integrative viewpoint. Network models with neuromorphic components are likely to possess greater information processing capabilities than the models studied at present. This leads to the question: what minimal properties of real neurons would be required to construct such networks? If ionic channels, neural transmitters, neural regulators, and neuronal geometry are all crucial factors governing electrical signaling, then the key point is to show how the connectivity among individual neurons brings about a coherent functional response. In other words, a way must be sought to bridge the gap between the various levels of the neural hierarchy, especially between the cellular, network, and systems levels.

19.5 Conclusions and Future Perspectives

In this chapter we have presented an analytical solution for a system of equations describing a model of a recurrent neuronal network. Further work is needed to extend the modeling to large-scale neuronal networks. Hasselmo and Kapur (2001) in their attempt at modeling large-scale neural networks wrote: "realistic models must take advantage of single cell properties beyond what is already simulated in an integrate-and-fire model." In this vein, the methodology presented herein goes beyond the older approaches such as the use of binary neurons to investigate dendritic integration in recurrent networks (Ascoli, 2003) or the population density utilizing "average neurons" (integrate-and-fire model neurons) to simulate large-scale neuronal networks (e.g., Haskell et al., 2001; Alvarez and Vibert, 2002; Toth and Crunelli, 2002; Renart et al., 2004).

Many examples of biological neural processing have been highly optimized through the action of evolution. Appreciation of the underlying algorithms is considered to be a valuable step towards implementing artificial systems of equivalent or better functionality. The opportunities for exploiting biological design in man-made systems have increased greatly with the development of very

large-scale integrated (VLSI) circuits in neurochips and other automata design. The possibility of uncovering new design principles can emerge from a program involving realistic modeling. The long-term focus of this research will be the foundation of biologically plausible large-scale neural networks focusing on the inclusion of the relevant biophysical processes, enabling the neurobiology of semantics to capture the essence of what will constitute "neuromimetic robotics" as the final frontier of modeling in the neurosciences.

ACKNOWLEDGMENTS

The author would like to thank G.N. Reeke, R.J. MacGregor S. Hidaka, and G.A. Chauvet for valuable discussions. I am indebted to Imperial College Press for permission to reproduce earlier work published in the *Journal of Integrative Neuroscience*.

PROBLEMS

1. On hippocampal CA1 pyramidal cells, synaptic plasticity (i.e., the strengthening and weakening of synaptic connections) has been shown to involve the movement of ligand-gated α-amino-3-hydroxy-5-methyl-4-isoxazoleproprioniate (AMPA) receptors (Baringa, 1999). Long-term potentiation (LTP) involves a modification to a synapse that depends on a relationship between the level of presynaptic activity and postsynaptic activity. This phenomenon can be accomplished by modifying Equation (2.6) with M^* now a function of presynaptic voltage, that is, $M^*[V\text{pre}(t)]$. Investigate whether LTP is observed in the model.
2. Extend the simulations to include repetitive firing (i.e., $j > 1$) of the presynaptic signals.
3. Consider a large-scale neuronal network consisting of realistic neurons represented by spatially distributed units (or dendritic cables without ionic channels), functionally connected in groups of neural assemblies (see Figure 19.7). Investigate the functional connectivity of such a system by extending the scalar analysis to matrix analysis. Derive an analytical solution in terms of Green's function matrices for a large-scale simulation of approximately 10,000 neurons arranged as a two-dimensional array of cortical columns. Obtain the integrated membrane potentials arising from spiking activity in the dendrites of such simulated neuronal networks. (Hint: Compute $e^{\mathbf{A}t}$ by finding the eigenvalues of $\mathbf{A}t$ where $\mathbf{A}$ is an $n \times n$ diagonal matrix and utilize the corollary given in Tuckwell [1988c]).
4. An extension to a large-scale recurrent neuronal network model will require an extensive use of matrix algebra and Green's function matrices. This type of research is still in its infancy and would represent an enormous leap forward over the models employed today. Determine Green's function matrices for a system of neuronal cables with ionic channels by taking Laplace transforms and obtaining a linear system of coupled ordinary differential equations.

APPENDIX: THE GREEN'S FUNCTION FOR A PASSIVE CABLE

The Green's function for a passive cable, $G^i(x, x_0; t), i = 0, 1$ corresponds to the response at time t and location x to a unit impulse at location x_0 at time $t = 0$ and is given by the solution to the following initial-value problem:

$$C_m G^i_t(x, x_0; t) = (d_i/4R_a)G^i_{xx}(x, x_0; t) - G^i(x, x_0; t)/R_{mi}, \tag{19A.1a}$$

$$G^i(x, x_0; 0) = \delta(x - x_0). \tag{19A.1b}$$

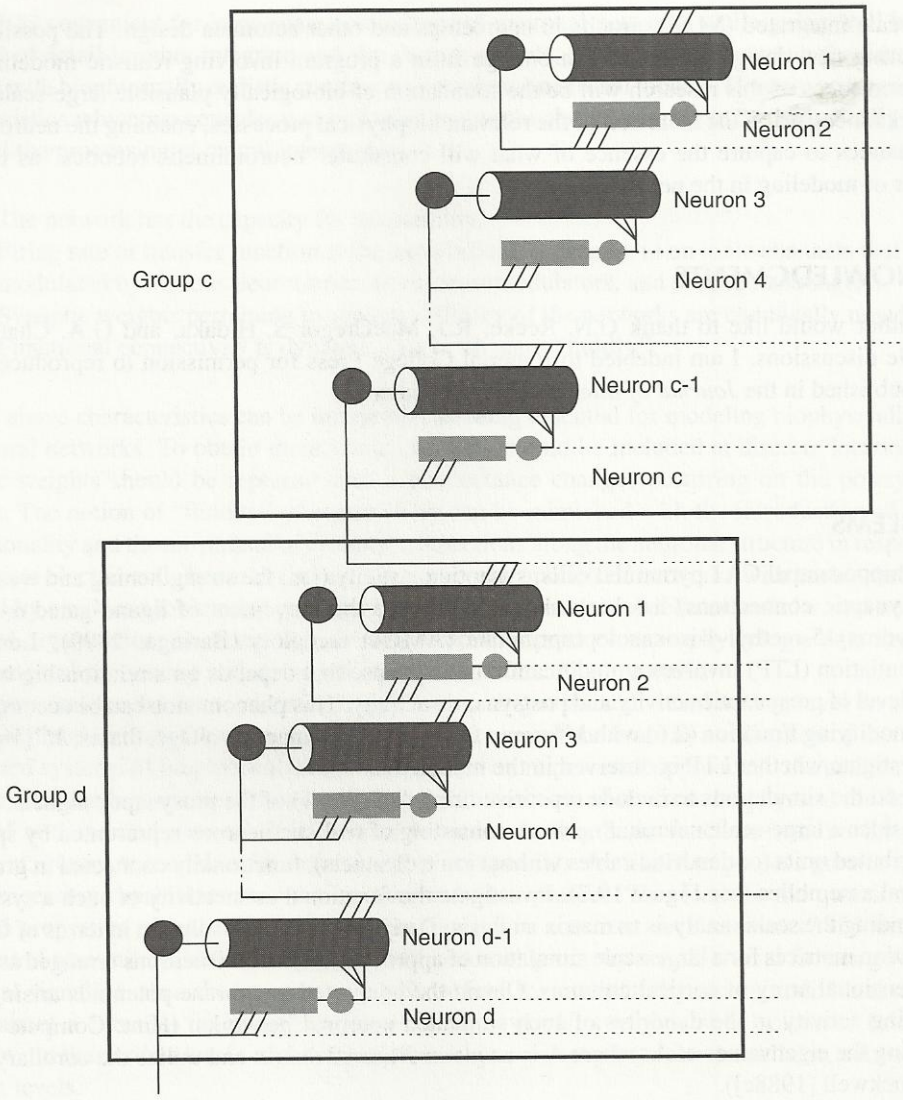

FIGURE 19.7 A schematic illustration showing a large-scale recurrent excitatory network of two neuronal groups located in different cortical areas (cf. Izhikevich et al., 2004). (*Source:* From R.R. Poznanski, ed, *Biophysical Neural Networks*, 2001b. With permission.)

For a single finite cable of length L_i with both ends sealed (i.e., $G_x^i(0, x_0; t) = G_x^i(L_i, x_0; t) = 0$), a representation that converges quickly for large t values was given by Tuckwell (1988a):

$$G^i(x, x_0; t) = (R_{mi}/L_i)\Bigg[\exp(-t/\tau_{mi}) + 2\sum_{n=1}^{\infty}\cos(n\pi x/L_i)\cos(n\pi x_0/L_i) \times \exp[-\{1 + (n\lambda_i\pi/L_i)^2\}(t/\tau_{mi})]\Bigg], \quad t > 0, \tag{19A.2}$$

where $\tau_{mi} = R_{mi}C_m$ and $\lambda_i = (R_{mi}d_i/4R_a)^{1/2} = (r_{mi}/r_a)^{1/2}$. An alternative representation that converges more quickly at small t values was also given by Tuckwell (1988a):

$$G^i(x, x_0; t) = (R_{mi}/\lambda_i)\exp(-t/\tau_{mi})\sqrt{(\tau_{mi}/4\pi t)}$$
$$\times \Big\{ \exp[-\tau_{mi}(x - x_0)^2/4\lambda_i^2 t] + \exp[-\tau_{mi}(x + x_0)^2/4\lambda_i^2 t]$$
$$+ \sum_{n=1}^{\infty} [\exp[-\tau_{mi}(x - 2nL_i - x_0)^2/4\lambda_i^2 t] + \exp[-\tau_{mi}(x - 2nL_i + x_0)^2/4\lambda_i^2 t]$$
$$+ \exp[-\tau_{mi}(x + 2nL_i - x_0)^2/4\lambda_i^2 t] + \exp[-\tau_{mi}(x + 2nL_i + x_0)^2/4\lambda_i^2 t]] \Big\}. \tag{19A.3}$$

For a single finite cable of length L_i with a lumped soma attached to the end at $x = 0$ (i.e., $G^i(0, x_0, t) + G_t^i(0, x_0, t) - \rho G_x^i(0, x_0, t) = 0$, where ρ is the dendritic-to-somatic conductance ratio), and with a sealed end at $x = L_i$ (i.e., $G_x^i(L_i, x_0, t) = 0$), a representation that converges quickly for large t values was also given by Tuckwell (1988a):

$$G^i(x, x_0; t) = (R_{mi}/\lambda_i)\exp(-t/\tau_{mi}) \sum_{n=0}^{\infty} \varphi_n^i(x) A_n^i(x_0) \exp[-(\psi_n^{i2} t/\tau_{mi})], \quad t > 0, \tag{19A.4}$$

where $\varphi_n^i(x) = \cos(\psi_n^i x/\lambda_i) - (\psi_n^i/\rho)\sin(\psi_n^i x/\lambda_i)$. The eigenvalues, ψ_n^i, are the roots of $\rho\tan(\psi_n^i L_i/\lambda_i) + \psi_n^i = 0$, and the coefficients are $A_n^i(x_0) = 2\rho\cos\theta_n/[\sin\psi_n^i L_i/\lambda_i\{(\rho/\psi_n^i - \psi_n^i L_i/\lambda_i) + (\rho/\lambda_i)(x_0 - L_i)\tan\theta_n\} + \cos\psi_n^i L_i/\lambda_i\{(2 + \rho L_i/\lambda_i) + \theta_n\tan\theta_n\}]$ and $A_0^i(x_0) = \rho/(1 + \rho L_i/\lambda_i)$, where $\theta_n^i = (x_0 - L_i)/\lambda^i\psi_n^i$ and $n = 1, 2, \ldots$. A representation that converges quickly for small t values can be found in Tuckwell (1988a).

For current injection at the end of the cable or at the soma, as opposed to injection along the cable, which reflects current density per unit length, it can be shown that the Green's function (G^{*i}) is simply $\lambda_i^{-1}G^i$, where G^i corresponds to the Green's function defined in (19A.2)–(19A.4).